

Assessment of Synaptic Function During Short-Term Facilitation in Motor Nerve Terminals in the Crayfish

M. Desai-Shah¹, K. Viele², G. Sparks¹, J. Nadolski³, B. Hayden¹, V.K. Srinivasan¹ and R.L. Cooper^{*1}

¹Department of Biology, Univ. of Kentucky, Lexington, KY., USA 40506-0225; ²Department of Statistics, Univ. of Kentucky, Lexington, KY, USA 40506-0027; ³Department of Mathematics and Computer Science, Benedictine University, Lisle, IL, 60532, USA

Abstract: An enhanced buildup of $[Ca^{2+}]_i$ occurs during short-term facilitation (STF) at the crayfish neuromuscular junction (NMJ). As a model system, this NMJ allows discrete postsynaptic quantal events to be counted and characterized in relation to STF. Providing 10 pulses, at 20 and 40Hz, we monitored postsynaptic quantal events over a discrete region of a nerve terminal with a focal macropatch electrode. Characteristics of quantal events were clustered into groups by peak amplitude and time to the peak amplitude. Since the synapses at this NMJ have varied spacing of active zones, number of active zones and synaptic size, the graded nature of synaptic recruitment is likely one means of titrating synaptic efficacy for the graded depolarization on the non-spiking muscle fiber. Synapses in this preparation would appear to have a "quantal signature" that can be used for quantifying their activity which is useful in estimating the overall number of active sites. We use mixture modeling to estimate n (number of active sites) and p (probability of vesicle fusion) from the quantal characteristics. In a preparation that was stimulated at 40Hz, synapses were recruited (increase in n) and the number active synapses increased in p . In a different preparation, p increased as the stimulation was changed from 20 to 40Hz, but n did not show a substantial increase; however, during the STF train, p increases slightly. This study provides a novel approach in determining subsets of the single evoked quanta to better estimate n and p which describe synaptic function.

INTRODUCTION

For nervous systems to function properly at various levels of excitation and inhibition, the efficacy of synapses is finely regulated and able to adjust in response to changing circumstances and requirements. However, unregulated variation in synaptic input when needing to relay a specific amount of information would provide an inappropriate signal for target cells to integrate. Due to the relative inaccessibility of postsynaptic dendrites and complexity of the central nervous system in general, most of our understanding in synaptic properties at a quantal level has been gained by studying accessible and relatively simple preparations, such as neuromuscular junctions (NMJ) [1-4]. Historically, the frog neuromuscular junction was used, but in physiological conditions the electrical events, due to nerve stimulation, produce action potentials that are conducted along the muscle. Further studies with lowered extracellular calcium or Ach-receptor blockers allowed more detailed studies to be made on the quantal nature of synaptic transmission [5]. Neuromuscular preparations in many invertebrates also serve as good models to investigate mechanisms underlying synaptic transmission since the postsynaptic evoked events are graded and do not spike, much like the dendrites of neurons in the vertebrate CNS. The advantage of NMJs is that the sites of release are able to be directly monitored without worrying about distortion due to electrical cable properties when

recording in a cell body within a CNS preparation. NMJs within crayfish were investigated particularly for these purposes [6-19].

Since synaptic strength is defined as the effectiveness of neurotransmission between pre- and post-synaptic cells, both pre- and post-synaptic factors can influence synaptic strength. Short-term plasticity of synapses, such as short-term facilitation (STF) which is a form of memory at a synaptic level, allows the gain of the system to be readily regulated without changing the hard wiring. In order to characterize transmission during STF, indexing the probability (p) and number of release sites (n) is valuable [10, 20, 21]; however, to measure n and p over time when the basal amount of release is changing is a difficult task by conventional methods [5, 22, 23].

Classically, the analysis of quantal release and estimation of p comes from the average probability of release over time, but since each quantal occurrence is counted as an event regardless of its size or shape of the postsynaptic response, this masks truly distinct synaptic sites. The traditional counting method would deem any two quantal events as identical in probability and site for release, even if the two currents (or potentials) appear distinctly different in their characteristics. Since differences in size or shape of the quanta are likely indicators that different synaptic sites are active, this can be useful information in determining if there is a change in the overall number of active sites during experimental manipulation [23]. Given that many synapses have been serially reconstructed for the crayfish opener excitatory NMJ, the nature of synaptic size and its synaptic complexity are becom-

*Address correspondence to this author at the Department of Biology, University of Kentucky, Lexington, KY., 40506-0225, USA; E-mail: RLCOOP1@email.uky.edu

ing well known [7, 10, 11, 24-26]. Direct structure-function studies of discrete regions of motor nerve terminals have revealed that there can be many synapses, each with multiple active zones. Physiological measures of quantal synaptic currents and field potentials along with estimation of n & p for low frequency stimulation (1Hz) reveals $n=1$ despite quite large variations in the size and shape of single evoked synaptic currents. The physiological and structural data would indicate that multiple sites are being utilized for vesicle fusion. In addition, the standardized approach of obtaining n and p from methods of directly counting quantal events [5] and determining their distribution of occurrence underestimates the functional number of sites. For these reasons, in an earlier study, we devised a means that incorporates differences in characteristics in the single quantal responses to estimate n and p for quantal subsets [23, 27, 28]. We now extend this analysis to the quantal responses during STF to estimate discrete n s and to assign a p to each given site. This type of analysis is a significant improvement over traditional analysis in determining the quantal parameters of release with multiple sites of release.

This work was presented previously in abstract form [29].

MATERIALS AND METHODOLOGY

General

All experiments were performed using the first and second walking legs of freshly obtained crayfish, *Procambarus clarkii*, measuring 6-8 cm in body length (Atchafalaya Biological Supply Co., Raceland, LA). The animals were housed individually in an aquatic facility and fed dried fish food. Dissected preparations were maintained in crayfish saline, a modified Van Harreveld's solution [30]. Crayfish were induced to autotomize the first or second walking leg by forcefully pinching at the merus segment.

Physiology

To elicit an evoked response, the excitatory axon was selectively stimulated by placing a branch of the leg nerve (from the merus segment) into a suction electrode connected to a Grass stimulator [31]. STF was induced by giving a train of pulses at 10 second intervals at 20 or 40Hz to the excitatory nerve. Intracellular EPSP and field EPSP (fEPSP) recordings were performed by standard procedures [8, 15, 30, 32]. The fEPSPs were recorded by placing a focal recording electrode directly over a visualized varicosity on the nerve terminal. A vital fluorescent dye, 4-[4-(diethylamino) styryl]-N-methylpyridinium iodide (4-Di-2-Asp; Molecular Probes, Eugene, OR), was used to visualize the varicosities [7, 33]. All chemicals were obtained from Sigma chemical company (St. Louis, MO). Electrical signals were recorded on-line to a PowerLab/4s interface (ADInstruments, Australia).

Direct counts of the number of evoked quantal events in evoked release were used as an index of synaptic function. If only a single event occurred after the spike, it was counted as one; when double events occurred, they were counted as two, and so on. In this study, 1000 trials of 10 pulses each were collected and recorded. An acquisition rate of 20kHz was used. The quantal events were individually examined to see whether they were single, double or more events. Mean quantal content (m) was determined by directly counting the

events [8]. For determining characteristics in the shape of quantal events, only discrete single events were used. In some cases, an event might ride on top of another event or start with very short synaptic delay and thus would lead to errors in separating out the signal of the action potential spike, produced by the nerve terminal in the recording, from the quantal event. Since multiple events could be counted as "events", they were used to determine mean quantal content but could not be used for assessment in the shape of the quantal event due to uncertainty in the true shape of the single event. Only distinct single events were processed for determining clusters of similar quantal properties.

Computational Analysis

The data points for the single evoked quanta were copied from the full traces and placed into individual columns within an Excel spreadsheet. The data points for each quanta were bracketed by the beginning of the quantal rise until the event returned to baseline. The files were transferred to text files. The routines herein are implemented in a statistical language called "S" using the freeware software "R" (R Development Core Team, 2005; see footnote). "R" is maintained by a consortium of statisticians and others, and may be downloaded at <http://www.r-project.org/>. We computed the time to the peak amplitude and peak amplitude for each single quanta within 500 traces for one experiment at 40Hz. In another experiment, 241 traces for 20Hz and 200 traces for 40Hz train stimulations. Each stimulation train consisted of 10 stimulation pulses at the given frequency. To determine the number of active sites and the firing rate for each site (n and p) over the course of the ten pulses, we employed normal mixture models similarly to Viele *et al.* [23]. A normal mixture model attempts to cluster observations into separate normal (Gaussian) distributions. Mixture models are commonly used in model-based clustering [34]. As with Viele *et al.* [23], we selected the number of normal distributions required based on Bayesian Information Criteria (BIC, [35]). This is a Bayesian procedure which consistently estimates the correct number of components, meaning that as the sample size increases BIC will choose the true underlying number of components. Instead of a p-value measuring "statistical significance", BIC can be calibrated by "posterior probabilities" which measures the relative likelihood the data reflect each possible number of components. For more information, see Kass and Raftery [35] or Gelman *et al.* [36]. In our context, differing components indicate differing active sites (in theory they could also mean the same site is having a different pattern of firing).

We performed the mixture analysis on the square root of the product of time to peak and peak amplitude. While at first this may seem an odd choice, it is justified in the literature. Previously, Viele *et al.* [23] clustered the square root of the area under the curve (AUC) measures, with the square root justified by the intuitive notion that area is measured in squared units, and the statistical justification that the square root transformation produced better fits. Note here the AUC values were difficult to compute because the small amount of time between pulses made the baseline computation difficult. While this issue also affects peak amplitude, in the AUC any baseline error is multiplied over the length of the trace. Viele *et al.* [28] demonstrated that AUC and the product of peak amplitude and rise time were highly correlated

(in that paper $\rho=0.96$). Thus, our response of interest is \sqrt{RP} , where R is the time to peak amplitude and P is the peak amplitude. Note that mixture models are invariant to affine transformations of the data, thus the units are irrelevant to the number of components estimated.

For the data from each of the 10 pulses, we fit normal mixture models of 1, 2, 3, and 4 components using the EM algorithm [37]. We then computed the BIC value for each of the four fits (BIC is a combination of the likelihood with a penalty term based on the number of parameters). These BIC values were then converted to posterior probabilities [35] and the model with the highest posterior probability was chosen. Thus, for each of the ten pulses, we chose one of 1, 2, 3, or 4 components.

For the best fitting model, we also recorded the fitted mean and variance of the normal distribution components and the estimated probability of firing. These best fits were then compared across the ten pulses to look for recruitment or changes in the active sites during STF.

RESULTS

The EPSP responses obtained by intracellular recordings show a marked facilitation at 40Hz stimulation within the 10 pulse stimulus train (Fig. 1, see **A1** panel). The average of 20 trials shown here replicates the general trend of single trains (Fig. **1B**). There are differences in the degree of facilitation depending on the region of the opener muscle that is being monitored [7, 38]. In this study, the terminals from central muscle fibers were used. It has been established that the majority of the facilitation during the STF is due to presynaptic components, primarily by enhanced calcium build up [39-42]. This build up of residual $[Ca^{2+}]_i$ enhances vesicular fusion and as expected mean quantal content [30]. To index the degree of enhancement, we calculated mean quantal content (m) by counting the discrete number of evoked quantal responses for each stimulus pulse within the 10 pulse train for each trial. Fig. (2) shows a representative trail of the individ-

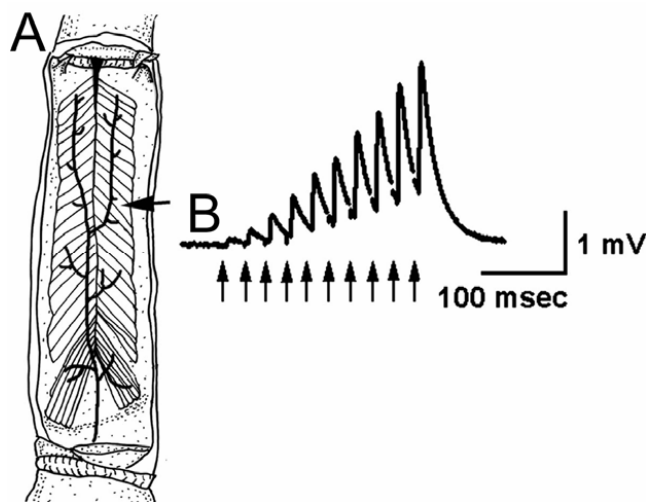


Fig. (1). (A) A schematic of the opener muscle in the crayfish walking leg showing the EPSP in response to a train of ten stimulation pulses given at 40Hz. (B) The EPSP responses recorded intracellularly from the central muscle fibers and the response shows a marked facilitation that occurs throughout the stimulation train. Arrows indicate each stimulation in the 10 pulse train.

ual fEPSP responses of a preparation stimulated at 40Hz with 10 pulse trains depicting the discrete quantal events recorded with a focal macropatch electrode over an identified region of the nerve terminal (Fig. **A1**). In some pulses, single evoked quantal events are observed while in others, the failure of evoking a response or even two quantal events is observable. The probability of multiquantal responses is relatively low during the initial part of the stimulus train but increases toward the tenth pulse. However, the range in the area and peak amplitudes of the single quantal events from the earlier pulses covers the same range as what are deemed as single events for the tenth pulse, so we are confident in what is deemed a single or a doublet is accurate. In addition, the probability of vesicular fusion is still not extremely high for the tenth pulse so probabilistically one should not expect

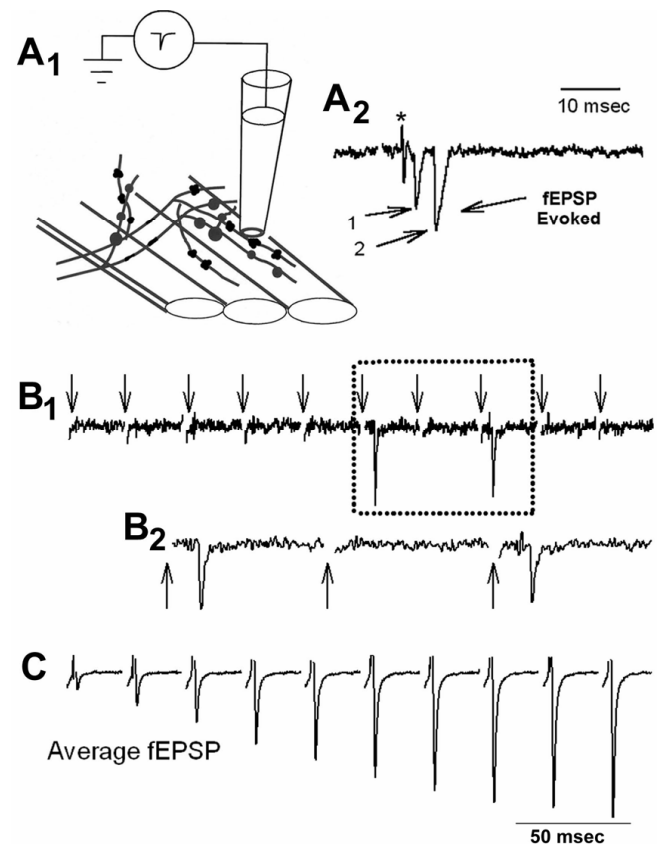


Fig. (2). (A1) Recordings of individual evoked quantal events are obtained by use of a focal macropatch electrode placed over visualized varicosity on a muscle fiber. (A2) The quantal responses (focal EPSP or fEPSP) from evoked release are monitored. The * shows the extracellular spike (action potential) preceding the quantal response. Two quanta are recorded here with a short latency between responses. (B1) Individual fEPSP responses depict the discrete quantal events. The 10 stimulation pulses are shown by arrows. The events 6 and 8 show single evoked quantal events. Failure to evoke an event is noted for the other pulses. (B2) The inset shows the enlarged time scale within the dotted box in trace **B1**. (C) The average field potential (fEPSPs) from 500 stimulation trails recorded over a single varicosity mimics the whole muscle EPSPs in facilitation of responses. The stimulus artifacts and the extracellular spikes were removed (blanks in the traces **B** and **C**) for ease of observing the evoked quantal events. The time scale bar shown in **C** is the same for the trace shown in **B1**.

Table 1. The discrete quantal counts for each pulse determined by direct observation. Mean quantal content (m) provides an index of presynaptic efficacy. All distributions in Fig. (3) at 40Hz were best fit by a poisson distribution so n and p are unrealistic to determine

Quanta	0	1	2	3	4	5	6	m
1st pulse	980	17	2	1	0	0	0	0.024
2nd pulse	946	51	3	0	0	0	0	0.057
3rd pulse	905	89	3	2	1	0	0	0.105
4th pulse	833	162	2	2	1	0	0	0.176
5th pulse	767	212	19	2	0	0	0	0.256
6th pulse	679	298	19	3	1	0	0	0.349
7th pulse	608	359	29	3	0	0	1	0.432
8th pulse	568	390	38	3	0	0	1	0.481
9th pulse	508	441	47	4	0	0	0	0.547
10th pulse	455	469	66	5	2	1	2	0.641

too many multiple events. The inset in Fig. (2A2) is a multi-quantal event with higher resolution. A 10 pulse series of stimuli are demarcated by the arrows in Fig. (2B1). The magnified region of the trace shown in Fig. (2B1) is depicted in Fig. (2B2) for clarity to demonstrate that multiple evoked events and failures in evoking a response can be resolved. The number of events associated for each pulse within the 10 pulse data set and m for each pulse are shown in Table 1. With the discrete counts, one can model various release probabilities (i.e., Binomial or Poisson). However, considering simultaneous estimation of n and p by discrete counts alone is notoriously unreliable and we had relatively low firing rates for many pulses we utilized functionals of the traces (e.g. peak amplitude, rise time, etc.) to estimate n and p . (see [23, 43, 44]; Olkin *et al.* [44] provides an example on how changing a single data point by 1 can change estimates of n by 100).

The rise in m over the pulse train is almost linear as shown with a linear least squares fit for one preparation examined at 40Hz (Fig. 3). In another preparation, m was calculated for each pulse at 20 and 40Hz stimulation trains (Fig.

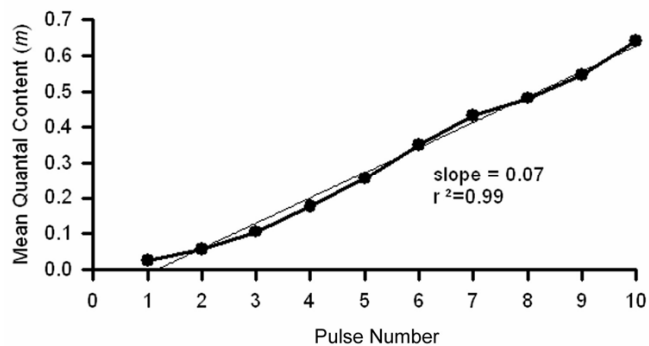


Fig. (3). Synaptic efficacy determined by m from direct counts throughout STF. The curve was fitted by a linear least squares fit and the R2 value is reported. This preparation was stimulated only at 40Hz.

4) and again a linear increase in m is observed for each stimulation frequency. This linearity may well change for different stimulation paradigms; however, with higher stimulation frequency the stimulus artifacts become mingled with the evoked responses which presents difficulty in obtaining measurements. Since the characteristics of each quantal event are used for further analysis, a good signal to noise ratio is required. The measures of the quantal events are illustrated on a single response in Fig. (5). The peak amplitude and rise time to peak were determined for each event that was deemed as a single event by direct observation. Once these measures were obtained, we proceeded with the various comparisons to examine novel quantal shapes that appeared to be recruited throughout STF.

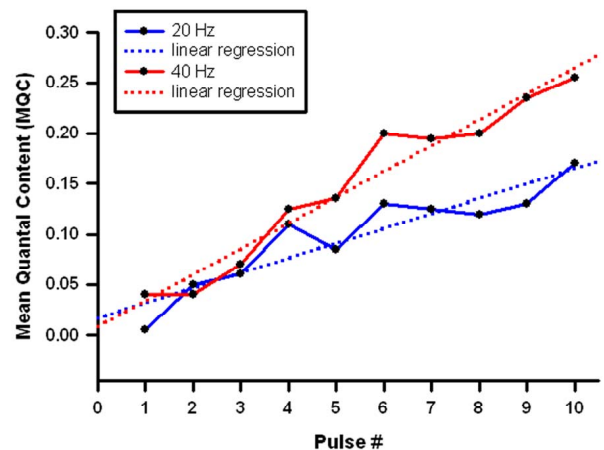


Fig. (4). Synaptic efficacy determined by m from direct counts throughout STF. The curve was fitted by a linear least squares fit. This preparation was stimulated at 20 and 40Hz. The linear least squares fit and the R2 values are: 20Hz is 0.85 and 40Hz is 0.95.

Table 2 shows the BIC values (in the left half of the table) for each pulse of the 1, 2, 3, or 4 potential fusion sites for the preparation depicted in Fig. (3) (40Hz alone). These BIC values have also been converted to Bayesian posterior

probabilities (in the right half of the table). Note BIC values are measured on the log scale, and thus their absolute difference, not relative difference, is important. Furthermore, BIC values are only comparable within each pulse, not across pulses as different pulses represent different datasets. For more information see [23, 35]. Values in bold indicate the best fit (the fit with the highest BIC and thus the highest posterior probability).

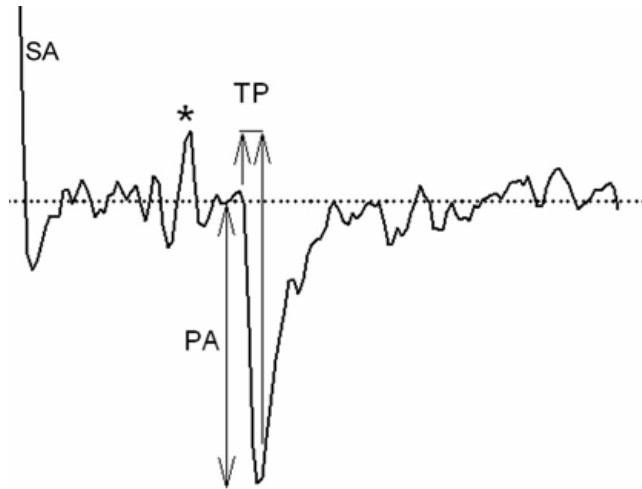


Fig. (5). The characteristic measures obtained from each quantal event are illustrated on this single response. The peak amplitude (PA) and the time to peak (TP) are shown. The stimulus artifact (SA) is followed by the extracellular spike (*) of the nerve terminal.

Table 3 summarizes the best fits for each of the ten pulses (preparation stimulated at 40Hz alone). For each fitted component, we report the mean μ (the fitted average value of $\sqrt{\text{RP}}$), the standard deviation σ , and the firing rate p (here p refers to the probability a stimulus results in a firing at that site for the specific pulse, thus the probabilities do not add to 1, instead they add to the overall firing rate for that pulse). Note the probability of firing is low for the first pulse and increases dramatically for higher pulses.

Fig. (6) shows the fits for these models. Each “pane” in Fig. (6) shows a histogram of the observed firings for one of the ten pulses. The individual estimated normal distributions are shown as either red, green, or blue curves. Finally, the black curve is the sum of the colored curves and provides the overall mixture fit to the histogram. As can be seen in the figure, all the mixture fits provide reasonable approximations to the observed histograms, including the multiple observed peaks for the data in some pulses.

The consistencies in Table 3 from pulse to pulse provide evidence concerning which sites are active at any given time. There is a site, active for pulses 1-8, with mean in the 0.45-0.60 range for $\sqrt{\text{RP}}$. The standard deviation for the results from this site is also consistent, ranging from 0.071-0.105. Note that the probability this site fires increases from a low 0.044 in pulse 1 to 0.408 in pulse 8. A second site appears to be recruited with a mean in the 0.728-0.817 range for $\sqrt{\text{RP}}$ for pulses 1-8. Finally, a third site is present for pulses 4-9 with a mean greater than 1. However, note this third site contains small probability and is typically represented by a small number of firings in each case (for example, probabilities of 0.01 correspond to 5 out of 500 traces).

It is quite unclear why the first site becomes inactive in pulses 9 and 10. It is also difficult to justify why the increasing probabilities of site 1 firing for pulses 1-8 suddenly drops to 0. Also, note that site 2 suddenly has a big jump in probability of firing going from pulse 8 to pulse 9, and a slight jump in standard deviation, possibly indicating the fitted results for sites 1 and 2 have combined (if two sites produce very similar patterns of firing, the mixture model will not be able to discriminate them). Finally, site 1 has an increasing trend in the mean. It is possible that the mean for site 1 increases to the point that in pulses 9 and 10, it is not possible to distinguish separate firing patterns for sites 1 and 2.

Similarly, it is unclear in pulse 10 why the 3rd site is any less active than it was in pulses 4-9. With such a low firing rate, it is possible that we simply did not observe a sufficient number or size of firing for the algorithm to detect.

Table 2. Bayesian information criteria values and estimated posterior probability for each of 1, 2, 3, and 4 component models fitted separately to the data from each pulse. Bold entries indicate the best fit for that pulse

Pulse	BIC1	BIC2	BIC3	BIC4	Pr(1)	Pr(2)	Pr(3)	Pr(4)
1	12.46	14.66	8.62	10.77	0.097	0.883	0.000	0.018
2	28.30	30.54	28.53	23.47	0.086	0.805	0.108	0.000
3	85.69	92.45	85.40	82.42	0.000	0.998	0.000	0.000
4	94.49	104.30	104.96	100.81	0.000	0.338	0.652	0.010
5	72.09	82.52	84.55	78.69	0.000	0.116	0.882	0.000
6	47.44	75.30	76.77	69.64	0.000	0.187	0.813	0.000
7	100.05	99.31	103.08	94.85	0.045	0.022	0.933	0.000
8	61.83	78.32	80.60	76.86	0.000	0.091	0.887	0.021
9	54.07	66.43	58.16	56.34	0.000	1.000	0.000	0.000
10	59.15	58.36	53.47	52.06	0.686	0.311	0.000	0.000

Table 3. Estimated means (μ), standard deviations (σ), and firing rates (relative to the total number of stimulations) for each normal density component (1, 2, or 3 indicating first, second, or third component) from the best fitting model for each pulse. The 1, 2, or 3 then relates to each potential release site. The results have been aligned in columns to indicate apparent similarity between the estimated components from pulse to pulse

	μ_1	σ_1	p_1	μ_2	σ_2	p_2	μ_3	σ_3	p_3
Pulse 1	0.444	0.088	0.044	0.782	0.010	0.004	-	-	-
Pulse 2	0.465	0.089	0.099	0.728	0.181	0.015	-	-	-
Pulse 3	0.454	0.071	0.189	0.615	0.146	0.081	-	-	-
Pulse 4	0.486	0.080	0.296	0.710	0.069	0.094	1.030	0.044	0.012
Pulse 5	0.496	0.089	0.293	0.718	0.134	0.231	1.145	0.301	0.012
Pulse 6	0.524	0.091	0.262	0.753	0.144	0.334	1.652	0.169	0.008
Pulse 7	0.580	0.101	0.350	0.817	0.120	0.264	1.465	0.022	0.004
Pulse 8	0.569	0.103	0.408	0.815	0.155	0.313	1.460	0.164	0.011
Pulse 9	-	-	-	0.704	0.190	0.672	1.993	0.010	0.002
Pulse 10	-	-	-	0.744	0.204	0.760	-	-	-

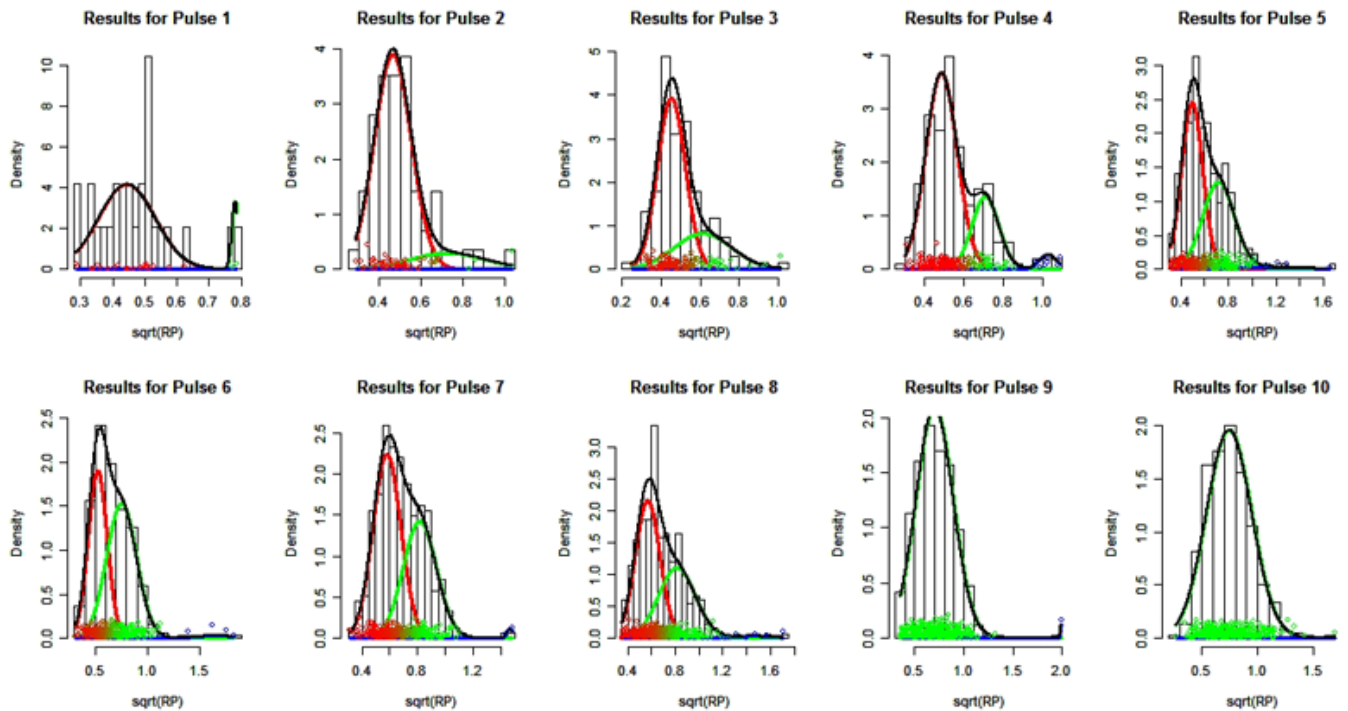


Fig. (6). Plots of the overall mixture fit and underlying fitted components for each of the ten pulses for 40hz (40hz only data).. Each histogram shows the sqrt(RP) data (square root of rise time multiplied by peak amplitude) for the corresponding pulse. The black line indicates the overall mixture fits, while the colored lines represent the underlying mixture components (the colored lines sum to the black line). The colored points indicate the estimated component membership of each data point. The y-axis “density” simply indicates the relative likelihoods of sqrt(RP) within each pulse.

Table 4. 20Hz data set for estimating BIC. Bayesian Information Criteria values and estimated posterior probability for each of 1, 2, 3, and 4 component models fitted separately to the data from each pulse. For pulses 1-3, an insufficient number of firings were recorded. Bold entries indicate the best fit for that pulse

Pulse	BIC1	BIC2	BIC3	BIC4	Pr(1)	Pr(2)	Pr(3)	Pr(4)
1	NA							
2	NA							
3	NA							
4	-107.1	-104.8	-104.3	-103.0	0.917	0.082	0.001	0.000
5	-110.4	-106.2	-108.5	-111.4	0.014	0.888	0.093	0.005
6	-148.3	-149.5	-146.8	-147.8	0.136	0.040	0.602	0.223
7	-148.8	-146.6	-145.9	-149.3	0.033	0.323	0.623	0.021
8	-144.5	-140.4	-144.7	-148.0	0.016	0.971	0.013	0.001
9	-155.6	-150.9	-155.0	-160.1	0.009	0.974	0.017	0.000
10	-194.6	-192.7	-193.7	-198.2	0.098	0.657	0.243	0.003

Table 5. Estimates of n and p for the pulses within the 20Hz train. Estimated means (μ), standard deviations (σ), and firing rates (relative to the total number of stimulations) for each normal density component (1, 2, or 3 indicating first, second, or third component) from the best fitting model for each pulse. The results have been aligned in columns to indicate apparent similarity between the estimated components from pulse to pulse

	μ_1	σ_1	p_1	μ_2	σ_2	p_2	μ_3	σ_3	p_3
Pulse 1	-	-	-	-	-	-	-	-	-
Pulse 2	-	-	-	-	-	-	-	-	-
Pulse 3	-	-	-	-	-	-	-	-	-
Pulse 4	86.45	10.64	0.095	-	-	-	-	-	-
Pulse 5	76.74	18.61	0.066	193.94	31.34	0.017	-	-	-
Pulse 6	72.45	16.59	0.082	141.65	45.56	0.019	119.91	1.05	0.020
Pulse 7	85.92	8.52	0.042	143.28	23.36	0.039	62.66	3.24	0.039
Pulse 8	68.40	12.17	0.079	136.89	29.29	0.038	-	-	-
Pulse 9	74.10	14.03	0.103	146.92	18.58	0.026	-	-	-
Pulse 10	86.61	17.95	0.137	161.23	18.31	0.025	-	-	-

For the preparation which was stimulated at 20 and 40Hz (Fig. 4), a similar analysis was performed for estimating the BIC values for each pulse of the potential fusion sites. These BIC values have been converted to Bayesian posterior probabilities for the 20Hz and 40Hz data (Table 4 and 6). The best fit parameters for each of the ten pulses (for the preparation stimulated at 20Hz and then at 40Hz) are shown in Tables 5 and 7. For each fitted components, we followed the same procedure as presented for the other preparation only stimulated at 40Hz with a mean μ , the standard deviation σ , and the firing rate p (here p refers to the probability a stimulus results in a firing at that site for the specific pulse). As with the other preparation, the probability of firing is low for the first pulse and increases dramatically slightly for higher pulses at both 20 and 40Hz stimulations. The graphs in Figs. (7) (20Hz) and (8) (40Hz) show the fits for the best fit models as in Fig. (6). In this particular preparation at 20Hz, there

were not enough quantal events for the first 3 pulses in the train to obtain any best fit model; even when the stimulation was turned up to 40Hz the initial pulses did not proved enough single events to fit well into any particular distribution. The model does predict that n was best described by 3 sites for the middle pulses within the train for 20Hz stimulation but then dropped back to 2 sites for later pulses; however, the p values are higher for the 2 sites than the earlier pulses within the train. A similar phenomenon was observed for the 40Hz with n changing slightly but p increasing slightly for each n with the increasing number of pulses within the stimulation train.

DISCUSSION

In this study, we have shown that there is an effect on synaptic efficacy during STF by enhancement of presynaptic fusion of vesicles, and the underlying nature for the increase

Table 6. 40Hz data set for estimating BIC. Bayesian Information Criteria values and estimated posterior probability for each of 1, 2, 3, and 4 component models fitted separately to the data from each pulse. For pulses 1-4, an insufficient number of firings were recorded. Bold entries indicate the best fit for that pulse

Pulse	BIC1	BIC2	BIC3	BIC4	Pr(1)	Pr(2)	Pr(3)	Pr(4)
1	NA							
2	NA							
3	NA							
4	NA							
5	-120.1	-116.4	-113.1	-113.2	0.001	0.018	0.516	0.465
6	-189.6	-190.4	-195.1	-200.2	0.687	0.310	0.003	0.000
7	-169.4	-168.4	-172.5	-175.6	0.274	0.714	0.012	0.001
8	-162.0	-160.1	-160.9	-165.7	0.100	0.606	0.292	0.002
9	-203.2	-198.9	-199.2	-202.6	0.008	0.549	0.430	0.014
10	-213.6	-209.0	-211.9	-215.8	0.010	0.936	0.053	0.001

Table 7. Estimates of n and p for the pulses within the 40Hz train. Estimated means (μ), standard deviations (σ), and firing rates (relative to the total number of stimulations) for each normal density component (1, 2, or 3 indicating first, second, or third component) from the best fitting model for each pulse. The results have been aligned in columns to indicate apparent similarity between the estimated components from pulse to pulse

	μ_1	σ_1	p_1	μ_2	σ_2	p_2	μ_3	σ_3	p_3
Pulse 1	-	-	-	-	-	-	-	-	-
Pulse 2	-	-	-	-	-	-	-	-	-
Pulse 3	-	-	-	-	-	-	-	-	-
Pulse 4	-	-	-	-	-	-	-	-	-
Pulse 5	63.47	9.16	0.095	147.25	4.48	0.010	98.65	1.69	0.020
Pulse 6	77.39	32.29	0.190	-	-	-	-	-	-
Pulse 7	71.46	15.04	0.175	139.80	8.53	0.010	-	-	-
Pulse 8	63.21	13.57	0.159	123.66	17.04	0.016	-	-	-
Pulse 9	66.17	11.90	0.204	122.41	16.31	0.021	-	-	-
Pulse 10	67.48	13.10	0.218	130.74	16.16	0.017	-	-	-

appears to be due to both an increase in probability of release from low threshold release sites as well as a recruitment of new release sites. Understanding the subtleties of synaptic transmission related to the function and recruitment of synaptic sites in close proximity is problematic due to the spatial resolutions and 3D nature of nerve terminals.

One would predict differences in the mechanisms of synaptic plasticity during STF depending on the synaptic architecture. Many synapses in the vertebrate CNS and NMJs appear to have a grid of presynaptic dense bodies, which are presumed to be active zones (AZ), spread out on the synaptic surface [45]. Thus, with such a structure, it is feasible to assume that each site has an equal probability of release during a given frequency of stimulation and either a tuning-up or -down the probability of the entire grid occurs during STF. Perhaps, there are exceptions for the AZs along the edge of

the synapse due to the lack of overlapping calcium clouds from neighboring AZs. However, synapses at the crayfish NMJ show a varied structural complexity with various sizes of synapses, numbers of AZs, as well as spacing among AZs. Such complexity is observed in insects and crustaceans [7, 9, 24] and has been vital to understanding synaptic plasticity to account for mutational effects in synaptically relevant issues in the *Drosophila* NMJ model [46].

Since the synapses occur on all sides of the terminal and are not planar, optical imaging by use of vesicle associated uptake dyes, such as FM1-43, would not allow optical assessment of multiple synapses simultaneously in these terminals. However, a physiological measure that characterizes discrete synapses at a quantal level is one possibility to assess multiple sites during STF as approached in this study. The variety in quantal responses has allowed us to

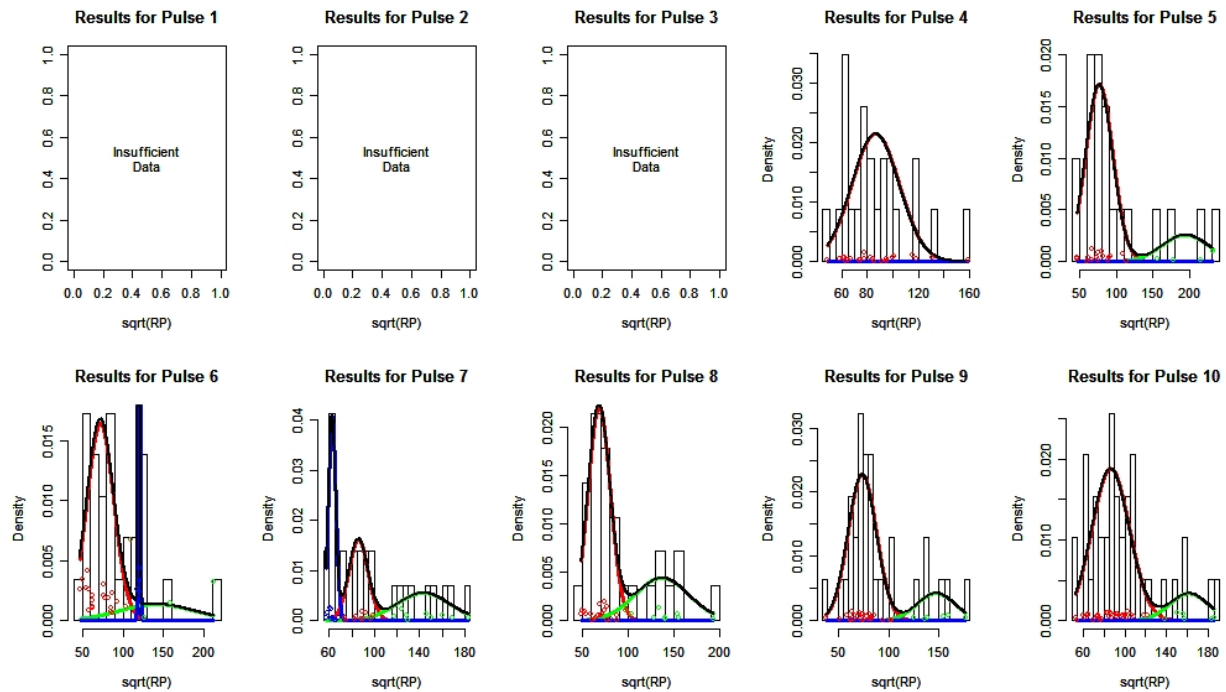


Fig. (7). Plots of the overall mixture fit and underlying fitted components for each of the ten pulses during 20Hz pulse train. Each histogram shows the sqrt(RP) data (square root of rise time multiplied by peak amplitude) for the corresponding pulse. The black line indicates the overall mixture fits, while the colored lines represent the underlying mixture components (the colored lines sum to the black line). The colored points indicate the estimated component membership of each data point. The y-axis “density” simply indicates the relative likelihoods of sqrt(RP) within each pulse.

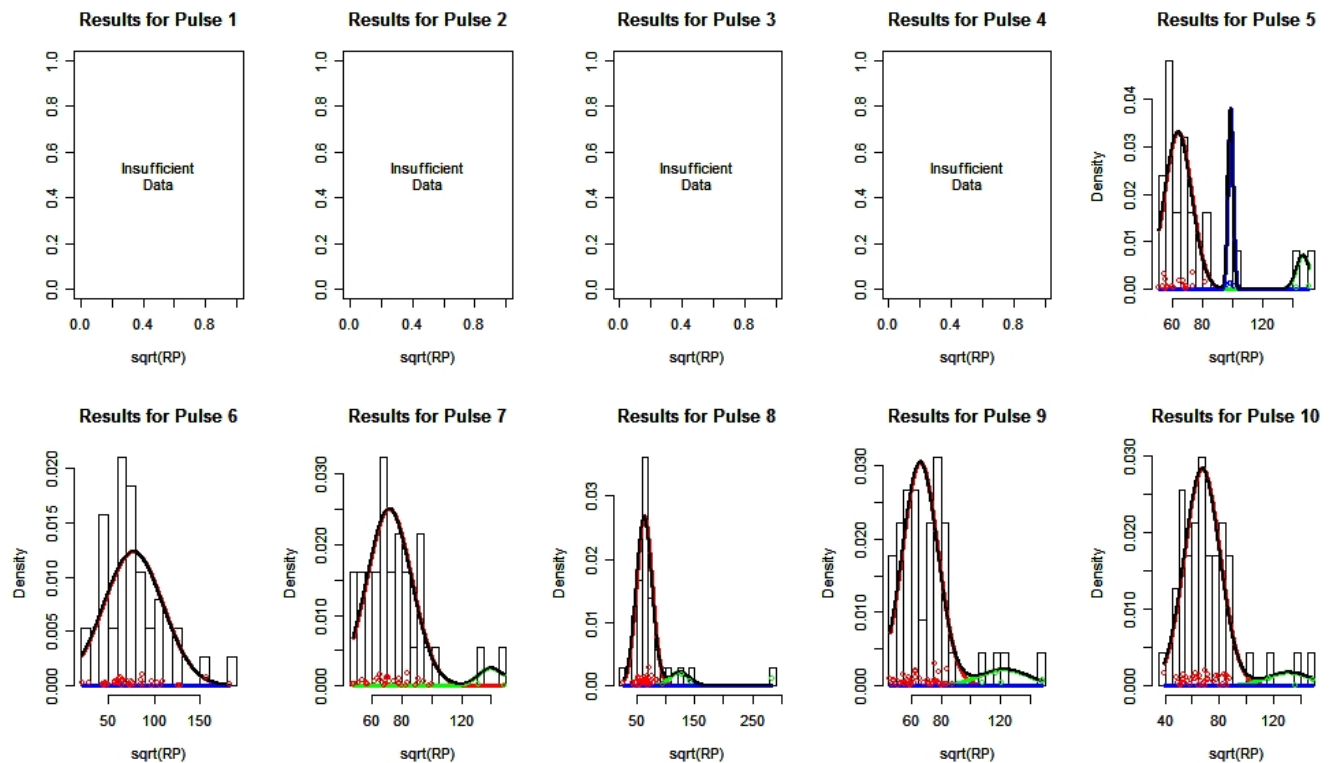


Fig. (8). Plots of the overall mixture fit and underlying fitted components for each of the ten pulses during 40Hz pulse train. Each histogram shows the sqrt(RP) data (square root of rise time multiplied by peak amplitude) for the corresponding pulse. The black line indicates the overall mixture fits, while the colored lines represent the underlying mixture components (the colored lines sum to the black line). The colored points indicate the estimated component membership of each data point. The y-axis “density” simply indicates the relative likelihoods of sqrt(RP) within each pulse.

group the quantal parameters for assessment in probability of occurrence and if new groupings appeared during STF. The analysis indicates that the overall rate of observing a firing increases for each successive pulse. In the preparation stimulated at 40Hz, only 3 active sites appear to have been used during the entire stimulus train. Sites 1 and 2 are active throughout pulses 1-8 (and site 1 is quite possibly active but not detectable in pulses 9-10), while site 3 is recruited at pulse 4. The results of the analysis also show that site 3 produces large values of $\sqrt{\text{RP}}$, but fires at a low rate. The other preparation, which was also stimulated for 10 pulses but at 20 and 40Hz, revealed that increasing the stimulation frequency increased the p more so than the n which accounted for the increase in m throughout the pulse train. The p increased for site 1 as compared to site 2. Given that a varicosity at this crayfish NMJ contains on the order of 20 to 40 synapses, it is surprising that n was not estimated to be higher during these pulse trains. Since there is such a linear increase in m within the pulse trains for both preparations (40Hz alone and for the one stimulated at 20 and then 40Hz), we would have expected the same in the estimated n and p values with this analysis. This suggests that the quantal counting method and the method presented herein are not directly comparable. Also, these results could suggest that quantal signatures are not likely to be present for discrete synapses by this means of analysis. We also expected that the results for the 40Hz stimulation among the two preparations would have produced more similar results in estimates for n and p among the pulses since both recordings were made from primary varicosities along the nerve terminal string of varicosities [10].

A potential error in these measures is a non-uniformity in size of vesicles that could produce varied size and shape of quantal responses for a given synapse; but since the synaptic vesicle diameters in the opener motor nerve terminal show little variation in size [47], we are fairly convinced that size does not account for the quantal variation observed. In addition, it is not likely that the rapidly recycling pool of vesicles did not have enough time to refill with glutamate in between pulse trains as this preparation can withstand being stimulated at 5Hz continuously for up to an hour before showing reduced quantal responses with use of a blocker for the pre-synaptic glutamate transporter [48]. In fact, the range in quantal responses for any given pulse appears to be maintained throughout the experimental paradigm used in this current study. Recently it was noted that *Drosophila* larvae, which are highly active crawlers, showed larger vesicles to appear after about 90 minutes of active crawling and that these vesicles were formed due to activity but became depleted over time [49]. If this was the case for the stimulation paradigm used in our study, then we would expect to show increased variation over time in the quantal responses for the 1st evoked pulses, which is not the case. Since the variation seen for each pulse is fairly consistent over time, but more variation occurs among different pulses (i.e., the 4th to the 8th) within a given train, indicates stability in recruiting similar threshold synapses. Recently, studies have shown that with high frequency stimulation, vesicles can be endocytosed by a bulk process thus allowing a large number of vesicular fusion events to occur at the synapses but without distorting the synaptic area [50]. In high-output NMJs of the crayfish on the extensor muscle, we did not observe bulk endocytosis

with prolonged stimulation in a recent study [51], so we would not expect to find bulk endocytosis during these relatively short pulse trains for the low-output NMJs used in this current study.

Some variation in the probability of release over the pulse train could be induced due to glutamate-ergic autoreceptor presynaptic feedback [52]. However, this should not influence the characteristic quantal shape but the likelihood of occurrence (i.e. p). Such feedback regulation on the pre-synaptic terminal could, in part, cause the plateau in the EPSP amplitudes from the underlying leveling off in the mean quantal content within long pulse trains, such as 20 or 40 pulses, delivered at 40Hz.

One source of error in our study is the latency between two simultaneous events. The timing might be short enough to produce a large response that is multi-quantal. Such errors would likely occur in the later pulses of the stimulus train when the probability is enhanced. A means to possible address this issue would be to reduce the $[\text{Ca}^{2+}]_o$ or to decrease the bath temperature in order to shift the synapses to a lower probability. In our study, we essentially changed the internal calcium by changing the stimulus frequency under the same external concentration. Such an approach was recently used to demonstrate in rat hippocampal neurons that the endocytic capacity is linked to the level of $[\text{Ca}^{2+}]_i$ [53]. Thus, with an increase of p for fusion within the STF train, there also needs to be an increase in the p of endocytosis. Similar studies of interest would be to document at the crayfish NMJ because of the large synaptic size and the known varied synaptic complexity differences for high- and low-output terminals at the NMJs [6].

In this study, we tested if a lateral shift occurs in n and p obtained at the beginning of the pulse train to the later stimulus pulses within the train as $[\text{Ca}^{2+}]_i$ is raised by starting off with 20Hz and then moving to 40Hz. Within the stimulus train of 10 pulses, there was an incremental increase in both n and p as the stimulus train increased for the same given stimuli within the train. In one recording the p increased substantially while n only varied by a value of 1 or 2. Currently, studies are underway to cause an earlier shift of n and p within the pulse train by raising $[\text{Ca}^{2+}]_i$ through blocking the sodium-calcium exchanger (NCX) [54].

The phenomenon commonly observed in the amplitude of EPSPs reaching a plateau during STF has not been fully addressed, but the balance in the influx through voltage gated channels, extrusion of calcium by pumps and the NCX are candidates because of a rapid time frame (100s of msec) [55]. In the STF induced in this study, the plateau is sub-maximal since a higher stimulation frequency results in yet higher amplitudes of EPSPs which reaches a new plateau. Thus, additional AZs would likely be recruited and the probability of the ones active at lower stimulation frequency would increase. When might all the AZs be recruited for a maximal n to be achieved? When this does happen, only the variation in the probability of each n will be increased for enhancing the gain of the system. However, if saturation in recruiting all the sites occurs at these NMJs is not known. With the analysis technique we present, it might be possible to address such issues.

Presenting another means for examining the quantal nature of synaptic transmission opens novel avenues for further investigating the mechanisms of synaptic function. Studies are currently underway in the lab with similar methodical approaches at the *Drosophila* NMJs in mutant strains related to synaptic function and glutamate receptor sensitivity.

FOOTNOTE

R: A language and environment for statistical computing. R Development Core Team R Foundation for Statistical Computing, Vienna, Austria 2005; ISBN 3-900051-07-0; <http://www.R-project.org>

ACKNOWLEDGMENTS

Funding was provided by NSF grants IBN-9808631 & ILI DUE-9850907 (R.L.C. & K.V.) and P 20 RR16481 from the National Center for Research Resources (NCR), a component of the National Institutes of Health (NIH)(KV).

G. Ribble Fellowships for undergraduate studies in the School of Biological Sciences at the University of Kentucky (BH; GS; VKS) and an Undergraduate Research Scholarship awarded by the Arnold and Mabel Beckman Foundation (GS).

REFERENCES

- [1] Bennett MR, Pettigrew AG. The formation of synapse in amphibian striated muscle during development. *J Physiol* 1975; 252: 203-39.
- [2] Nudell BM, Grinnell AD. Regulation of synaptic position, size and strength in anuran skeletal muscle. *J Neurosci* 1983; 3: 161-76.
- [3] Wilkinson RS, Lunin SD. Properties of "reconstructed" motor synapses of the garter snake. *J Neurosci* 1994; 14: 3319-32.
- [4] Wilkinson RS, Lunin SD, Stevermer JJ. Regulation of single quantal efficacy at the snake neuromuscular junction. *J Physiol* 1992; 448: 413-36.
- [5] Del Castillo J, Katz B. Quantal components of the end-plate potential. *J Physiol (Lond)* 1954; 124: 560-73.
- [6] Atwood HL, Cooper RL. Synaptic diversity and differentiation: Crustacean neuromuscular junctions. *Invert Neurosci* 1996; 1: 291-307.
- [7] Cooper RL, Marin L, Atwood HL. Synaptic differentiation of a single motor neuron: Conjoint definition of transmitter release, pre-synaptic calcium signals, and ultrastructure. *J Neurosci* 1995; 15: 4209-22.
- [8] Cooper RL, Stewart BA, Wojtowicz JM, Wang S, Atwood HL. Quantal measurement and analysis methods compared for crayfish and *Drosophila* neuromuscular junctions and rat hippocampus. *J Neurosci Methods* 1995; 61: 67-78.
- [9] Cooper RL, Hampson D, Atwood HL. Synaptotagmin-like expression in the motor nerve terminals of crayfish. *Brain Res* 1996; 703: 214-6.
- [10] Cooper RL, Harrington C, Marin L, Atwood HL. Quantal release at visualized terminals of crayfish motor axon: Intraterminal and regional differences. *J Comp Neurol* 1996; 375: 583-600.
- [11] Cooper RL, Winslow J, Govind CK, Atwood HL. Synaptic structural complexity as a factor enhancing probability of calcium-mediated transmitter release. *J Neurophysiol* 1996; 75: 2451-66.
- [12] Cooper RL, Ruffner ME. Depression of synaptic efficacy at intermolt in crayfish neuromuscular junctions by 20-Hydroxyecdysone, a molting hormone. *J Neurophysiol* 1998; 79: 1931-41.
- [13] Dudel J. Potential changes in the crayfish motor nerve terminal during repetitive stimulation. *Pflügers Arch* 1965; 282: 323-37.
- [14] Dudel J. The effect of reduced calcium on quantal unit current and release at the crayfish neuromuscular junction. *Pflügers Arch* 1981; 391: 35-40.
- [15] Dudel J, Parnas I, Parnas H. Neurotransmitter release and its facilitation in crayfish muscle. VI. Release determined by both, intracellular calcium concentration and depolarization of the nerve terminal. *Pflügers Arch* 1983; 399: 1-10.
- [16] Fatt P, Katz B. Distributed "End Plate Potentials" of crustacean muscle fibers. *J Exp Biol* 1953; 30: 433-9.
- [17] Fatt P, Katz B. The electrical properties of crustacean muscle fibers. *J Physiol* 1953; 120: 171-204.
- [18] He P, Southard RC, Whiteheart SW, Cooper RL. Role of α -SNAP in promoting efficient neurotransmission at the crayfish neuromuscular junction. *J Neurophysiol* 1999; 82: 3406-16.
- [19] Southard RC, Haggard J, Crider ME, Whiteheart SW, Cooper RL. Influence of serotonin on the kinetics of vesicular release. *Brain Res* 2000; 871: 16-28.
- [20] McLachlan EM. The statistics of transmitter release at chemical synapses. In: Porter R, Ed. *International Review of Physiology, Neurophysiology III*, Baltimore, MD: University Park Press 1978; vol. 17: pp. 49-117.
- [21] Stricker C, Redman S, Daley D. Statistical analysis of synaptic transmission: Model discrimination and confidence limits. *Biophys J* 1994; 67: 532-47.
- [22] Korn H, Faber DS. Quantal analysis and synaptic efficacy in the CNS. *Trends Neurosci* 1991; 14: 439-45.
- [23] Viele K, Stromberg AJ, Cooper RL. Estimating the number of release sites and probability of firing within the nerve terminal by statistical analysis of synaptic charge. *Synapse* 2003; 47: 15-25.
- [24] Atwood HL, Cooper RL. Functional and structural parallels in crustaceans and *Drosophila* neuromuscular systems. *Am Zool* 1995; 35: 556-65.
- [25] Atwood HL, Cooper RL. Assessing ultrastructure of crustacean and insect neuromuscular junctions. *J Neurosci Methods* 1996; 69: 51-8.
- [26] Govind CK, Atwood HL, Pearce J. Inhibitory axoaxonal and neuromuscular synapses in the crayfish opener muscle: Membrane definition and ultrastructure. *J Comp Neurol* 1995; 351: 476-88.
- [27] Lancaster M, Viele K, Johnstone AFM, Cooper RL. Automated classification of evoked quantal events. *J Neurosci Methods* 2007; 159: 325-36.
- [28] Viele K, Lancaster M, Cooper R. The self-modeling structure of excitatory post-synaptic potentials. *Synapse* 2006; 60: 32-44.
- [29] Desai MS, Viele K, Hayden BJ, Cooper RL. Quantal release during short-term facilitation in motor nerve terminals of the crayfish. *Society for Neuroscience, Annual meeting, San Diego, CA. 2007* (abstract).
- [30] Sparks G, Cooper RL. 5-HT offsets homeostasis of synaptic transmission during short-term facilitation. *J Appl Physiol* 2004; 96: 1681-90.
- [31] Dudel J, Kuffler SW. The quantal nature of transmission and spontaneous miniature potentials at the crayfish neuromuscular junction. *J Physiol* 1961; 155: 514-29.
- [32] Crider ME, Cooper RL. Differential facilitation of high- and low-output nerve terminals from a single motor neuron. *J Appl Physiol* 2000; 88: 987-96.
- [33] Magrassi L, Purves D, Lichtman JW. Fluorescent probes that stain living nerve terminals. *J Neurosci* 1987; 7: 1207-14.
- [34] Raftery A, Dean N. Variable Selection for Model-Based clustering. *J Am Stat Assoc* 2006; 101: 168-78.
- [35] Kass R, Raftery A. Bayes Factors. *J Am Stat Soc* 1995; 90: 773-95.
- [36] Gelman A, Carlin J, Stern H, Rubin D. *Bayesian Data Analysis*, 2nd ed. Chapman and Hall 2004.
- [37] Dempster A, Laird N, Rubin D. Maximum likelihood from incomplete data via the EM algorithm. *J R Stat Soc Ser B* 1977; 39: 1-38.
- [38] Mykles DL, Medler SA, Koenders A, Cooper RL. Myofibrillar protein isoform expression is correlated with synaptic efficacy in slow fibres of the claw and leg opener muscles of crayfish and lobster. *J Exp Biol* 2002; 205: 513-22.
- [39] Katz B, Miledi R. The role of calcium in neuromuscular facilitation. *J Physiol* 1968; 195: 481-92.
- [40] Rahamimoff R. A dual effect of calcium ions on neuromuscular facilitation. *J Physiol* 1968; 195: 471-80.
- [41] Winslow JL, Duffy SN, Charlton MP. Homosynaptic facilitation of transmitter release in crayfish is not affected by mobile calcium chelators: Implications for the residual ionized calcium hypothesis from electrophysiological and computational analyses. *J Neurophysiol* 1994; 72: 1769-93.
- [42] Zucker RS, Lara-Estrella LO. Post-tetanic decay of evoked and spontaneous transmitter release and a residual-calcium model of synaptic facilitation at crayfish neuromuscular junctions. *J Gen Physiol* 1983; 81: 355-72.

- [43] Casella G, Berger R. Statistical Inference, 2nd ed. Duxbury Press 2001.
- [44] Olkin I, Petkau AJ, Zidek JV. A comparison of n-estimators for the binomial distribution. J Am Stat Assoc 1981; 76: 637-42.
- [45] Atwood HL. Neuroscience. Gatekeeper at the synapse. Science 2006; 312: 1008-9.
- [46] Stewart BA, Schuster CM, Goodman CS, Atwood HL. Homeostasis of synaptic transmission in *Drosophila* with genetically altered nerve terminal morphology. J Neurosci 1996; 16: 3877-86.
- [47] Kim S, Atwood HL, Cooper RL. Assessing accurate sizes of synaptic vesicles in nerve terminals. Brain Res 2000; 877: 209-17.
- [48] Logsdon S, Johnstone AFM, Viele K, Cooper RL. Regulation of synaptic vesicles pools within motor nerve terminals during short-term facilitation and neuromodulation. J Appl Physiol 2006; 100: 662-71.
- [49] Steinert JR, Kuromi H, Hellwig A, *et al.* Experience-dependent formation and recruitment of large vesicles from reserve pool. Neuron 2006; 50: 723-33.
- [50] Clayton EL, Evans GJ, Cousin MA. Bulk synaptic vesicle endocytosis is rapidly triggered during strong stimulation. J Neurosci 2008; 28: 6627-32.
- [51] Johnstone AFM, Kellie S, Cooper RL. Presynaptic depression in phasic motor nerve terminals and influence of 5-HT on docked vesicles. Open Neurosci J 2008; 2: 16-23.
- [52] Dudel J, Schramm M. A receptor for presynaptic glutamatergic autoinhibition is a glutamate transporter. Eur J Neurosci 2003; 18: 902-10.
- [53] Balaji J, Armbruster M, Ryan TA. Calcium control of endocytic capacity at a CNS synapse. J Neurosci 2008; 28: 6742-9.
- [54] Desai-Shah M, Cooper RL. Roles of the Sodium Calcium Exchanger (NCX), the Plasma Membrane Ca²⁺-ATPase (PMCA) and the Sarcoplasmic/Endoplasmic Reticulum Ca²⁺-ATPase (SERCA) in synaptic transmission at the Crayfish and *Drosophila* Neuromuscular Junctions. Society for Neuroscience, Annual meeting, Washington DC, 2008 (abstract).
- [55] Juhaszova M, Church P, Blaustein MP, Stanley EF. Location of calcium transporters at presynaptic terminals. Eur J Neurosci 2000; 12: 839-46.

Received: March 13, 2008

Revised: May 02, 2008

Accepted: August 08, 2008

© Desai-Shah *et al.*; Licensee Bentham Open.

This is an open access article licensed under the terms of the Creative Commons Attribution Non-Commercial License (<http://creativecommons.org/licenses/by-nc/3.0/>) which permits unrestricted, non-commercial use, distribution and reproduction in any medium, provided the work is properly cited.